How Often Will It Rain?

YING SUN

National Climate Center, China Meteorological Administration, Beijing, China, and NOAA/Earth System Research Laboratory, Boulder, Colorado

SUSAN SOLOMON

NOAA/Earth System Research Laboratory, Boulder, Colorado

AIGUO DAI

National Center for Atmospheric Research, Boulder, Colorado*

ROBERT W. PORTMANN

NOAA/Earth System Research Laboratory, Boulder, Colorado

(Manuscript received 27 February 2006, in final form 16 January 2007)

ABSTRACT

Daily precipitation data from climate change simulations using the latest generation of coupled climate system models are analyzed for potential future changes in precipitation characteristics. For the Intergovernmental Panel on Climate Change (IPCC) Special Report on Emissions Scenarios (SRES) B1 (a low projection), A1B (a medium projection), and A2 (a high projection) during the twenty-first century, all the models consistently show a shift toward more intense and extreme precipitation for the globe as a whole and over various regions. For both SRES B1 and A2, most models show decreased daily precipitation frequency and all the models show increased daily precipitation intensity. The multimodel averaged percentage increase in the precipitation intensity (2.0% K^{-1}) is larger than the magnitude of the precipitation frequency decrease (−0.7% K^{-1}). However, the shift in precipitation frequency distribution toward extremes results in large increases in very heavy precipitation events (>50 mm day^{-1}), so that for very heavy precipitation, the percentage increase in frequency is much larger than the increase in intensity (31.2% versus 2.4%). The climate model projected increases in daily precipitation intensity are, however, smaller than that based on simple thermodynamics (~7% K^{-1}). Multimodel ensemble means show that precipitation amount increases during the twenty-first century over high latitudes, as well as over currently wet regions in low- and midlatitudes more than other regions. This increase mostly results from a combination of increased frequency and intensity. Over the dry regions in the subtropics, the precipitation amount generally declines because of decreases in both frequency and intensity. This indicates that wet regions may get wetter and dry regions may become drier mostly because of a simultaneous increase (decrease) of precipitation frequency and intensity.

1. Introduction

As the climate warms, changes in precipitation characteristics, such as frequency, intensity, and duration, may occur. Tropospheric warming (e.g., due to increased greenhouse gases) leads to exponential increases in the water-holding capacity of the atmosphere by ~7% K^{-1}, which is largely governed by the Clausius–Clapeyron equation (Trenberth 1998; Semenov and Bengtsson 2002; Allen and Ingram 2002; Trenberth et al. 2003). With little change in relative humidity (e.g., Soden et al. 2002; Dai 2006a), this means exponential increases in atmospheric moisture content. Trenberth et al. (2003) argued that in a warmer climate, heavy precipitation intensity should increase at the same rate as for atmospheric moisture (i.e., ~7% K^{-1}) because

* The National Center for Atmospheric Research is sponsored by the National Science Foundation.

Corresponding author address: Ying Sun, National Climate Center, China Meteorological Administration, 46 Zhongguancun Nandajie, Beijing 100081, China.
E-mail: yingsun75@yahoo.com

DOI: 10.1175/JCLI4263.1

precipitation rates from storms are determined by low-level moisture convergence. Since the change in the overall intensity of the global hydrologic cycle (i.e., global evaporation or precipitation) is controlled by the availability of energy at the surface, not by the availability of moisture (Boer 1993; Allen and Ingram 2002), climate models predict that the intensity of the global hydrological cycle increases by about 1%–2% K^{-1} (Cubasch et al. 2001). The implication is that there must be a decrease in light or moderate precipitation and/or a decrease in the frequency of precipitation events (Trenberth et al. 2003).

Analyses of historical precipitation records generally show disproportionate increases of heavy or intense precipitation during the last several decades over the United States (Karl and Knight 1998; Kunkel et al. 2003; Groisman et al. 2004), Europe (Klein Tank and Können 2003), Southeast Asia (Manton et al. 2001), and other land areas (Groisman et al. 2005), although the analyses are not always conclusive (e.g., Haylock and Nicholls 2000). Some model studies have shown a general increase in precipitation intensity and a decrease in the number of wet days with increased greenhouse gases (e.g., Gordon et al. 1992; Hennessey et al. 1997). Cubasch et al. (2001) and more recent studies (e.g., Wilby and Wigley 2002; Groisman et al. 2005; Meehl et al. 2005; Emori and Brown 2005; Emori et al. 2005) indicate that the increase in precipitation intensity remains a consistent result over many regions in improved, more comprehensive models. Wilby and Wigley (2002) suggest that the proportion of total precipitation derived from extreme and heavy events will continue to increase in the twenty-first century relative to moderate and light precipitation events. Emori and Brown (2005) found that atmospheric thermodynamics plays a dominant role in the difference between model-simulated mean and extreme precipitation changes, while atmospheric dynamics (i.e., circulation) has only a secondary effect. Other studies (e.g., Semenov and Bengtsson 2002; Watterson and Dix 2003) employed sophisticated statistical analyses, such as the gamma distribution, to examine potential changes in precipitation characteristics and extremes in some individual models, and they also found similar results.

Thus there exists both observational and model evidence that supports a key role for thermodynamic effects on the changes in precipitation characteristics in a warmer climate. However, climate change simulations from many of the latest generation of climate models have not been analyzed to validate these results. Furthermore, changes in the frequency and intensity of different categories of precipitation and their regional response to different emissions scenarios have not been analyzed from the viewpoint of multimodel ensembles.

Here we analyze monthly and daily precipitation data from 17 of the latest generation of coupled global climate models for changes in precipitation frequency and intensity for different precipitation categories under three future emissions scenarios. The focus here is on the common features of multimodel ensembles. We examine both the global and regional features of changes in precipitation characteristics and the consistency between the thermodynamic arguments (Trenberth et al. 2003) and the model projections. This study is a continuation of our previous work on model-simulated mean precipitation frequency and intensity under current climate conditions (Sun et al. 2006). The paper is organized as follows: section 2 describes the data and analysis method; section 3 reveals the change in precipitation distributions under the Intergovernmental Panel on Climate Change (IPCC) Special Report on Emissions Scenarios (SRES); sections 4–6 present, respectively, the global mean, zonal mean, and geographical distributions of changes in precipitation frequency and intensity for the two emissions scenarios; and section 7 provides a discussion and some conclusions.

2. Data and analysis method

The model precipitation-related data for current [1980–99, twentieth-century climate (20C3M)] and future (2080–99) climates under three emissions scenarios (SRES B1, with low emissions of greenhouse gases; A1B, a medium emissions projection; and A2, a high projection) were extracted from the IPCC simulations for the Fourth Assessment (AR4). The IPCC AR4 dataset consists of the outputs from the newest generation of coupled general circulation models (CGCMs) and has been archived at the Program for Climate Model Diagnosis and Intercomparison (PCMDI). Here monthly data from 17 models were used to analyze the changes in precipitation, precipitable water (PW), surface latent heat flux, and convective precipitation. Daily precipitation data from 14 models were employed for the analyses of precipitation frequency and intensity. The models are CGCM3.1(T47), CGCM3.1(T63), CNRM-CM3, CSIRO Mk3.0, GFDL CM2.0, GFDL CM2.1, GISS-ER, FGOALS-g1.0, INM-CM3.0, IPSL CM4, MIROC3.2(hires), MIROC3.2(medres), ECHAM5, MRI CGCM2.3.2, CCSM3, PCM, and UKMO-HadCM3. There is no daily data available in models CSIRO Mk3.0, MRI CGCM2.3.2, and UKMO-

TABLE 1. Percentage changes from 1980–99 to 2080–99 in globally averaged total precipitation amount (Pr), frequency (Freq), intensity (Inten), convective precipitation amount (Prc), and absolute changes in surface air temperature for SRES B1 scenario (Tas). The second column shows the letters used for different models in Figs. 3–5.

Model name	Model symbol	Pr (%)	Freq (%)	Inten (%)	Prc (%)	Tas (K)
CGCM3.1(T47)	A	3.28	0.05	3.14	0.88	1.58
CGCM3.1(T63)	B	4.46	0.44	3.92	3.00	2.16
CNRM-CM3	C	2.46	−0.34	3.23	1.86	1.61
CSIRO Mk3.0	D	1.84			1.79	1.07
GFDL CM2.0	E	3.41	0.17	3.14	0.76	1.98
GFDL CM2.1	F	2.14	−0.06	2.20	−0.72	1.56
GISS-ER	H	3.12	0.13	2.98	5.06	1.42
FGOALS-g1.0	K	2.10	0.66	2.43	2.56	1.64
INM-CM3.0	L	3.80	−0.57	4.69	6.44	1.97
IPSL CM4	M	4.92	−0.44	5.39	4.19	2.14
MIROC3.2(hires)	N	5.42	−0.90	6.86	6.08	3.07
MIROC3.2(midres)	R	3.74	−0.49	4.09	7.14	2.22
ECHAM5	S	4.20	−2.44	7.18	4.11	2.16
MRI CGCM2.3.2	T	3.35			4.14	1.48
CCSM3	W	3.92	0.55	3.85	4.86	1.54
PCM	X	4.69	0.22	3.67	5.41	1.42
UKMO-HadCM3	Z	2.08			2.48	1.91
Average		3.47	−0.22	4.06	3.53	1.82

HadCM3. The available models for SRES A2 are less than those for SRES B1. Tables 1 and 2 provide detailed information about the models used in the present paper. A description of the models can be found at http://www-pcmdi.llnl.gov/ipcc/about_ipcc.php. Additional information regarding precipitation parameterizations in these models is given in Dai (2006b) and Sun et al. (2006).

The gridded daily precipitation data (0.5° × 0.5°, 1980–99) derived from rain gauge records included in the Global Telecommunication System (GTS; P. Xie 2005, personal communication) were also used in the paper. This land daily precipitation dataset was derived by Xie et al. (1996) at the National Centers for Environmental Prediction (NCEP) from GTS precipitation reports (6000 stations) using the algorithm of Shepard (1968). In this paper, we averaged the 0.5° × 0.5° data onto a 3° × 3° grid (hereafter GTS_3D) for comparison with model precipitation.

In this study, we examined the continuous histograms of daily precipitation frequency and amount with a bin size of 1 mm day^{-1}. Precipitation amount in each bin is

TABLE 2. Same as in Table 1, except for SRES A2.

Model name	Model Symbol	Pr (%)	Freq (%)	Inten (%)	Prc (%)	Tas (K)
CGCM3.1(T47)	A	6.16	−0.43	6.39	0.65	3.18
CGCM3.1(T63)	B					
CNRM-CM3	C	5.13	−1.01	7.11	3.49	3.42
CSIRO Mk3.0	D	4.28			4.35	2.57
GFDL CM2.0	E	2.59	−0.78	2.52	−5.08	3.26
GFDL CM2.1	F	1.67	−0.79	2.35	−5.85	3.01
GISS-ER	H	4.90	−0.10	4.87	8.47	2.68
FGOALS-g1.0	K					
INM-CM3.0	L	5.49	−1.58	7.33	10.41	3.25
IPSL CM4	M	7.49	−1.51	8.62	4.43	3.53
MIROC3.2(hires)	N					
MIROC3.2(medres)	R	4.01	−1.28	5.41	6.85	3.61
ECHAM5	S	6.12	−4.04	12.02	5.54	3.49
MRI CGCM2.3.2	T	5.41			6.54	2.54
CCSM3	W	7.26	0.43	7.68	8.60	3.58
PCM	X	3.81	−0.006	4.24	4.10	2.27
UKMO-HadCM3	Z	2.78			2.92	3.28
Average		4.80	−1.0	6.23	4.00	3.12

the total (accumulated) precipitation amount per year for each bin. Furthermore, to facilitate the discussion of spatial variations, we also classified daily precipitation into a limited number of commonly used categories: very light (0.1–1 mm day^{-1}), light (1–10 mm day^{-1}), moderate (10–20 mm day^{-1}), heavy (20–50 mm day^{-1}), and very heavy (>50 mm day^{-1}) precipitation. There are other ways to define precipitation categories, such as using percentiles of a distribution or the return period of precipitation events under current climate. These two definitions provide slightly different angles to look at precipitation characteristics that account for spatial variations in mean precipitation. Since all the methods define the categories using fixed criteria based on current climate, they all show some migration of the precipitation events across fixed thresholds in a changing climate. This is true even when the percentile or return period method is used since they actually correspond to certain fixed precipitation intensity levels for current climate at each grid point. The migration across fixed thresholds is just one of the ways for the predefined events to change in a changing climate. Our continuous histograms, however, provide some context for judging this kind of migration. Using definitions similar to that used here, Sun et al. (2006) and Dai (2006b) show the distributions of precipitation frequency, intensity, and amount for various categories from observations and the IPCC AR4 models under current climate. Here we present model projected changes in these precipitation characteristics under the three warming scenarios.

Precipitation frequency was calculated by dividing the number of days with precipitation within an intensity interval or a precipitation category by the number of all days with data and expressed as a percentage. The mean precipitation intensity for each category was calculated as the mean precipitation rates averaged over the days with the corresponding precipitation events. In this paper, the future (2080–99) changes in all the variables are expressed percentage changes relative to present (1980–99) values. This makes the changes more comparable spatially and among models and simulations with differing mean climate states. There are other approaches to describe the changes, such as normalizing the data by the standard deviation of the time series (e.g., Meehl et al. 2005; Tebaldi et al. 2006) or scaling the results with global-mean precipitation change to exclude the effects of different climate sensitivity of the models and of different scenarios (Emori and Brown 2005). These different approaches should yield similar results regarding the sign and large-scale patterns of future precipitation changes.

3. Changes in precipitation histograms

Figure 1 shows the mean histograms of daily precipitation frequency (Fig. 1a) and amount (Fig. 1c) derived from observations (1980–99, GTS_3D) and 11-model ensemble simulations for the present (1980–99, 20C3M) and future (2080–99) climates under SRES B1, A1B, and A2 scenarios. The percentage changes for the future scenarios are shown in Figs. 1b and 1d. The observed daily precipitation are only available over land, so both land and global- (for models only) mean histograms are shown in Fig. 1. The land and global-mean histograms are derived by calculating the histogram (i.e., distributions) at each grid box and then averaging the histograms spatially. Figure 1 shows that the models overestimate the frequency for precipitation less than ~20 mm day^{-1} but underestimate the frequency for precipitation more than ~20 mm day^{-1}. Also, the amount of intense precipitation (>~20 mm day^{-1}) and its contribution to total precipitation amount are higher in observations than models (Fig. 1c). Figure 1 is consistent with previous finding that precipitation occurs too frequently at reduced intensity in climate models (e.g., Chen et al. 1996; Dai et al. 1999; Sun et al. 2006; Dai 2006b).

The multimodel ensemble (Fig. 1) shows a shift toward more frequent heavy precipitation and a larger amount of precipitation derived from these events under all three warming scenarios than the present. The highest emission scenario SRES A2 shows the largest change in the precipitation distributions for both global and land average. Figure 1 suggests increased risk of flash floods over land from increased intense precipitation under the SRES emissions scenarios. Examination of individual regions revealed similar shifts toward intense precipitation in the warmer climates.

The percentage increases in intense precipitation frequency and amount are large, with the greatest increase for under SRES A2. The increases are greater over land than for the globe, which implies a greater response of precipitation over land regions than the oceans to atmospheric greenhouse gas forcing.

Figure 2 shows the precipitation frequency distribution averaged over land for the individual models and from observations. With increased greenhouse gases, all the models consistently show increased frequency of heavy precipitation. However, the models considerably underestimate the observed frequency of heavy precipitation. One exception is the MIROC3.2(hires), which shows good agreement with the observations except in the segment from ~10 to ~40 mm day^{-1} in which the MIROC3.2(hires) overestimates the frequency. Sun et al. (2006) suggest that this model's relatively good per-

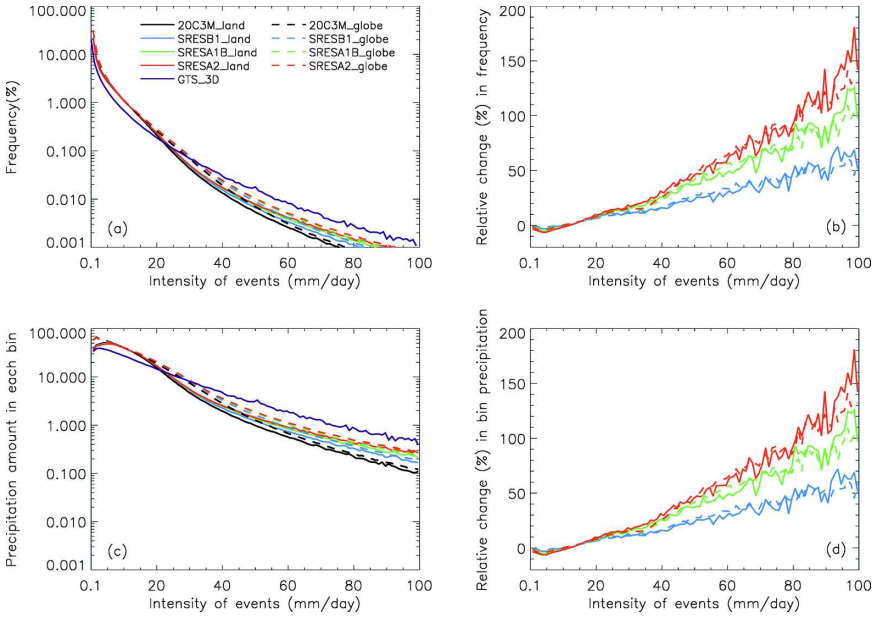

FIG. 1. (a) Globally (dashed line) and land- (solid line) averaged distribution of daily precipitation frequency as a function of precipitation intensity (bin size is 1 mm day^{-1}) from observations (GTS_3D, 1980–99) and an 11-model ensemble of simulations for present [twentieth-century climate (20C3M), 1980–99] and future (2080–99) climates under SRES B1, A1B, and A2 scenarios; (b) Same as in (a) but for percentage changes; (c) same as in (a), but for precipitation amount (mm) in each bin; and (d) same as in (c) but for percentage changes.

formance to reproduce intense precipitation may be due to an empirical cumulus suppression added to the Arakawa–Schubert scheme in this model.

4. Future changes in precipitation characteristics: Global average

Figure 3 shows the scatterplots of globally averaged percentage changes from 1980–99 to 2080–99 in precipitation, precipitable water, surface latent heat flux, and convective precipitation versus changes in global-mean surface air temperature for scenario SRES B1 (blue) and A2 (red). The global-mean surface temperature increases by 1.1–3.6 K and precipitation by 1.7%–7.6% for the two scenarios considered. A least squares fit to all the model data yields a slope of 1.2% K^{-1}, which is similar to previous estimates (e.g., Cubasch et al. 2001; Allen and Ingram 2002), but it is evident that certain models depart from the general behavior. Compared with the simulations with CO_2 forcing only (e.g., Cubasch et al. 2001), the intermodel scattering is large here, which may reflect the different effects of aerosols, especially their indirect effects in some of the models. If the results of models E, F, R, and Z under SRES A2 are excluded, the slope is 1.7% K^{-1}. The two GFDL models (E and F) show smaller precipitation increases in the warmer SRES A2 case than the B1 case (Fig. 3a), which results from decreases in convective precipitation in the SRES A2 case.

Global-mean precipitable water in the models increases linearly with the temperature at 9.1% K^{-1}, which is slightly higher than the rough thermodynamic estimate of ~7% K^{-1} (Trenberth et al. 2003). This may be partly explained as global warming by the reduction in the tropospheric temperature lapse rate in the Tropics. Bony et al. (1995) have shown that in climate warming experiments, the precipitable water variation in the Tropics is controlled by the variations not only in the surface temperature but also in the lapse rate and relative humidity profile. This is different from the dominant contribution of surface temperature to precipitable water variation in middle and high latitudes. Therefore, as global warming may occur, with little change in relative humidity, the extra contribution from the lapse rate reduction in the Tropics, which is not considered in the simple thermodynamic estimate, may increase atmospheric precipitable water for given surface warming. A reduction in the lapse rate is consistent with enhanced warming in the middle and upper troposphere found in most climate model projections (e.g., Cubasch et al. 2001; Dai et al. 2001a).

Most models show balanced increases in global-mean

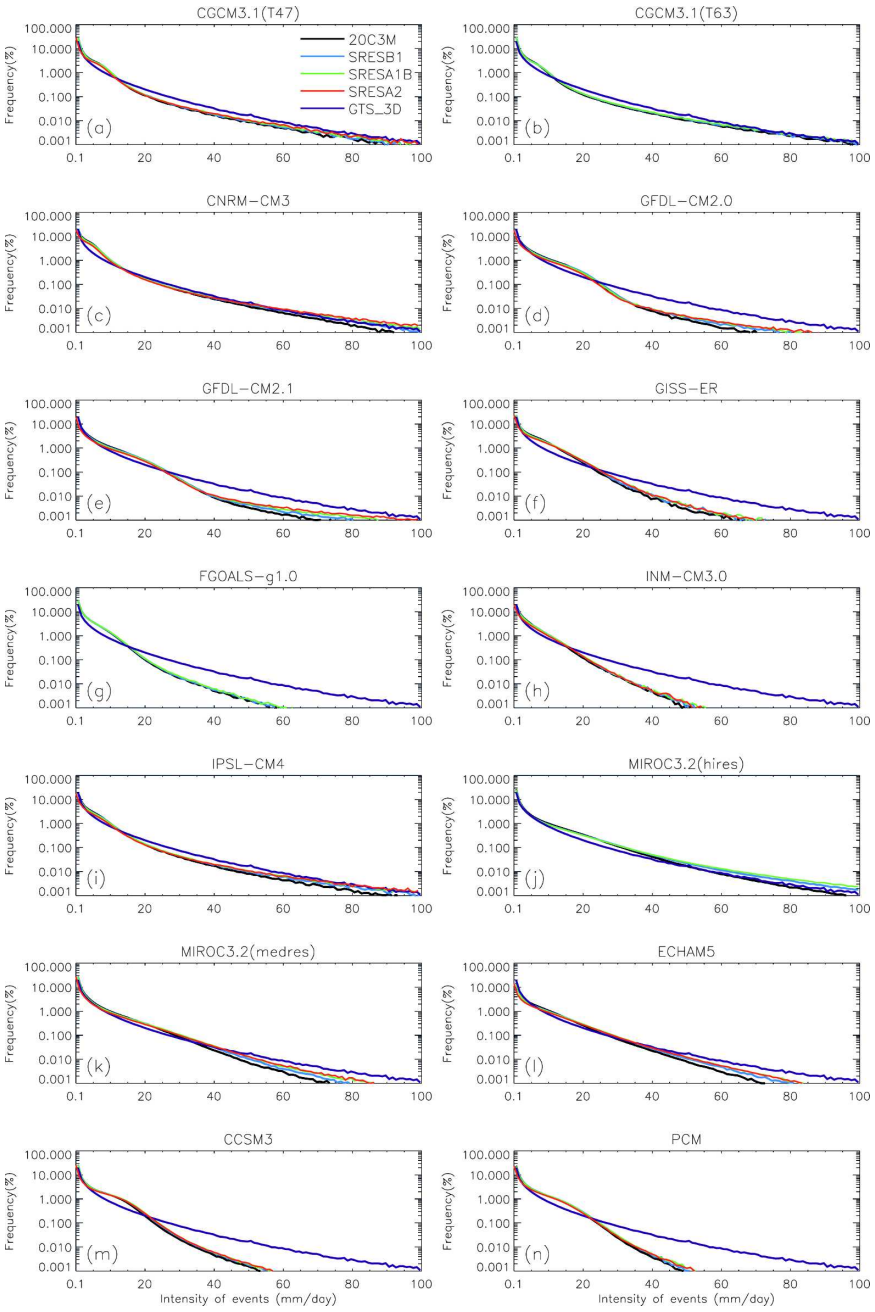

FIG. 2. Same as in Fig. 1a, but for 14 individual models.

precipitation (Fig. 3a) and evaporation (Fig. 3c, evaporation = latent heat flux ÷ L, where $L = 2.5 \times 10^6$ J kg^{-1} is the latent heat coefficient), which are expected as atmospheric water storage is small. The correlation between the changes in convective precipitation and the temperature is weak ($r = 0.13$), but convective precipitation generally increases with the temperature, except for the GFDL CM2.0 (E) and CM2.1 (F) models, which show smaller increases in both total and convective precipitation for SRES A2 than SRES B1. The reason for this abnormal behavior in the GFDL models is unknown.

Figure 4 shows the global-mean percentage change in precipitation frequency for different categories of precipitation as a function of global-mean temperature changes from 1980–99 to 2080–99. For all the precipitation events (>0.1 mm day^{-1}), the frequency changes are small under the SRES B1 scenario in all the models

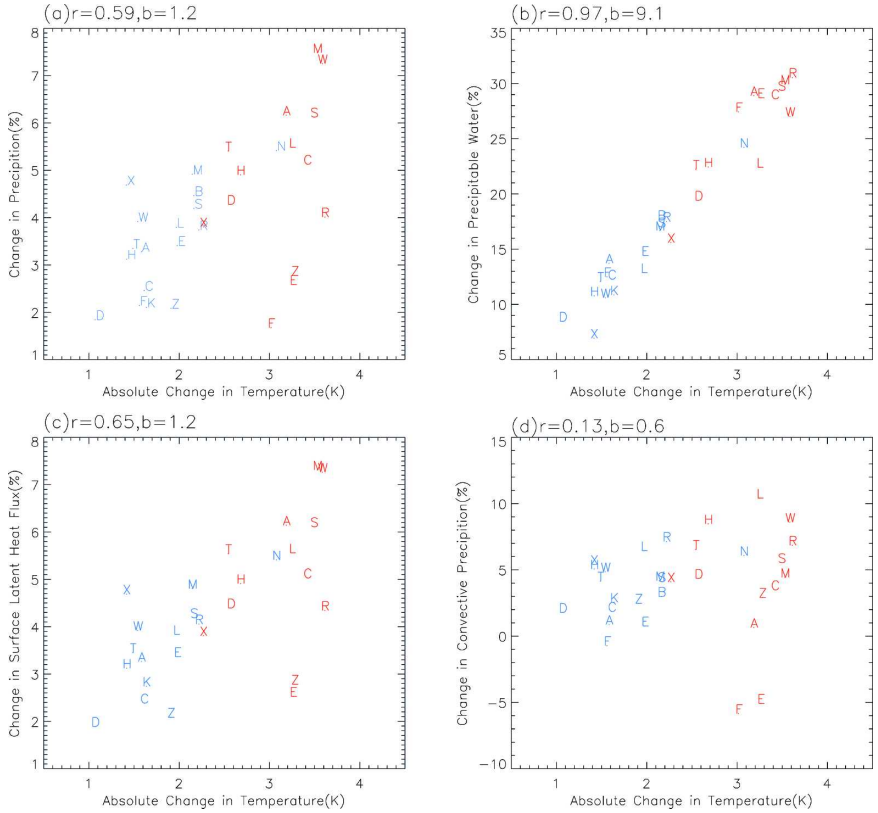

FIG. 3. Scatterplots of model-simulated percentage changes (%) from 1980–99 to 2080–99 in globally averaged, annual-mean (a) precipitation amount, (b) precipitable water, (c) surface latent heat flux, and (d) convective precipitation vs changes in global-mean temperature (K) under the SRES B1 (blue) and A2 (red) scenarios. Each letter denotes one model (see Table 1 for model names). The "r" and "b" indicate the correlation coefficients and regression slope, respectively. Precipitable water is not directly available in UKMO-HadCM3 (Z) and surface latent flux is not available in CGCM3.1(T63) (B) and GFDL CM2.1 (F).

except for ECHAM5 (S), which shows a decrease of 2.4% (Table 1). Under the warmer SRES A2 scenario, most models show slight decreases (~−1%) in the frequency, except for the CCSM3 (W), PCM (X), and GISS-ER (H) (Table 2; Fig. 2a). The CCSM3 shows slight increases (~0.5%) in the frequency under both scenarios, while the ECHAM5 shows the largest decrease (−4.04% in the SRES A2 case), which corresponds to the largest increase in the intensity (Fig. 5a). The difference in the sign of the frequency changes between A2 and B1 results is mainly from the regional response of precipitation frequency to different radiative forcing. Under the high emissions scenario SRES A2, the changes become more evident (not shown) over most regions due to its large radiative forcing. As shown below (cf. Fig. 10a), precipitation frequency decreases over most of mid- and low latitudes. As a result, the globally averaged frequency decreases under SRES A2 because of large area weight for these regions. This is true in all the models except for model W (CCSM3) (see Tables 1 and 2). The CCSM3 shows an unreasonable (too large) frequency change in northern Africa for reasons unknown. The present results imply that a simple pattern scaling cannot be applied for the two scenarios.

For very light and moderate precipitation (Figs. 4b,d), there is no consistent relationship between the changes in frequency and temperature. Changes in the frequency of light precipitation are small under the SRES B1 scenario and generally negative (about −2% to −5%) in the SRES A2 case (Fig. 4c). The similarity between changes in the total and light precipitation frequency (Figs. 4a,c) results partly from the large contribution of the light precipitation to the total precipitation. For most models, light precipitation contributes more than 40% to the total precipitation amount, which is too high compared with observations (Dai 2006b). For heavy precipitation frequency, most models show

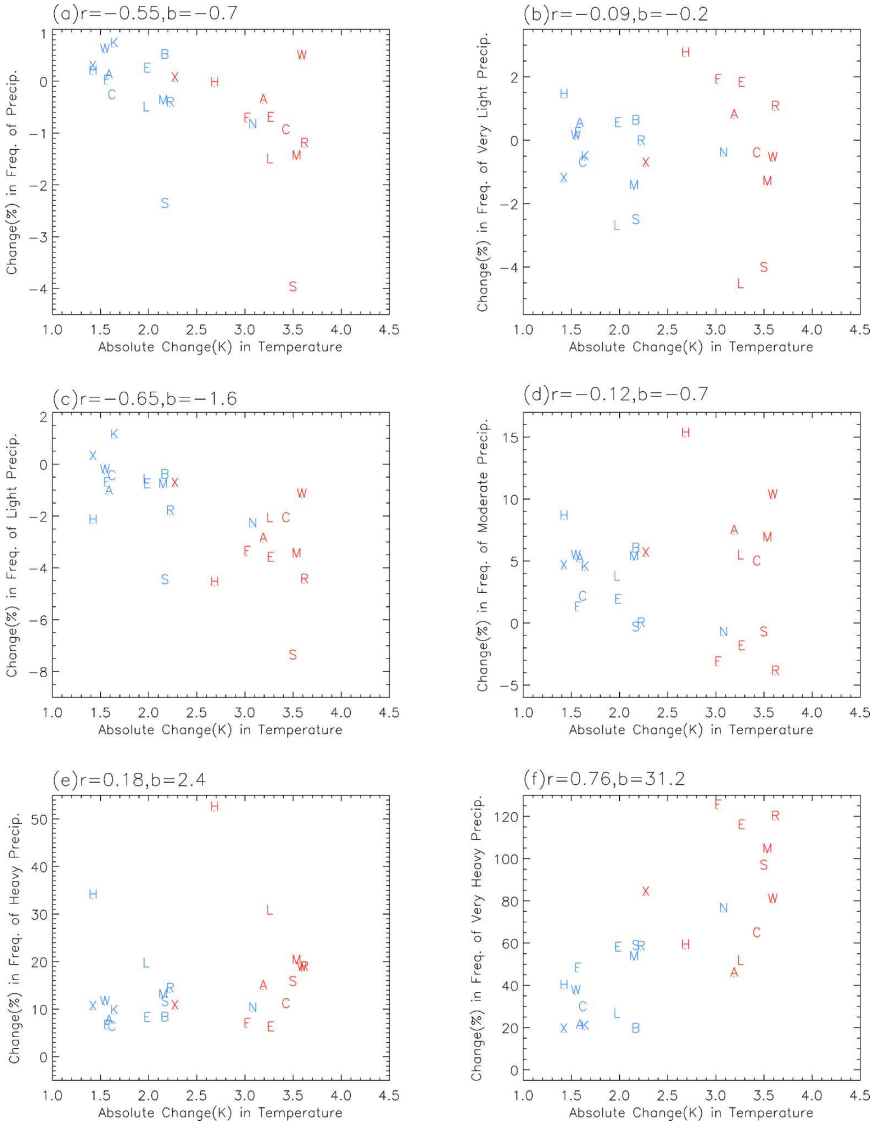

FIG. 4. Same as Fig. 3, but for the frequency of (a) all precipitation events (>0.1 mm day^{-1}), (b) very light (0.1–1.0 mm day^{-1}), (c) light (1–10 mm day^{-1}), (d) moderate (10–20 mm day^{-1}), (e) heavy (20–50 mm day^{-1}), and (f) very heavy (>50 mm day^{-1}) precipitation. Daily precipitation data are available only for 14 models under SRES B1 and for 11 models under SRES A2 (see Tables 1 and 2).

increases of 7%–16% for SRES B1 and 7%–21% for SRES A2 (Fig. 4e). The increase in frequency of very heavy precipitation is very large for most of the models, about 20%–60% for SRES B1 and 45%–125% for SRES A2, and it increases with surface warming (31.2% K^{-1}) (Fig. 4f). This trend of large percentage increases of frequency for heavy precipitation continues with precipitation events >100 mm day^{-1}. These events are only seen in the Tropics (~30°S–30°N) and the East Asian summer monsoon region in the models. The frequency change in these precipitation events (not shown) is very large, with increases of ~50%–300% for SRES B1 and ~100%–700% for SRES A2. The regression slope between temperature and the frequency change is 132.7% K^{-1} and correlation coefficient among the models is 0.69.

The changes in the intensity of daily precipitation (Fig. 5) are different to the above frequency changes. All of the models show increases in the intensity of all precipitation events for the two scenarios, at about 2.0% K^{-1}, with the two GFDL models (E and F) having similar intensity increases under the two scenarios

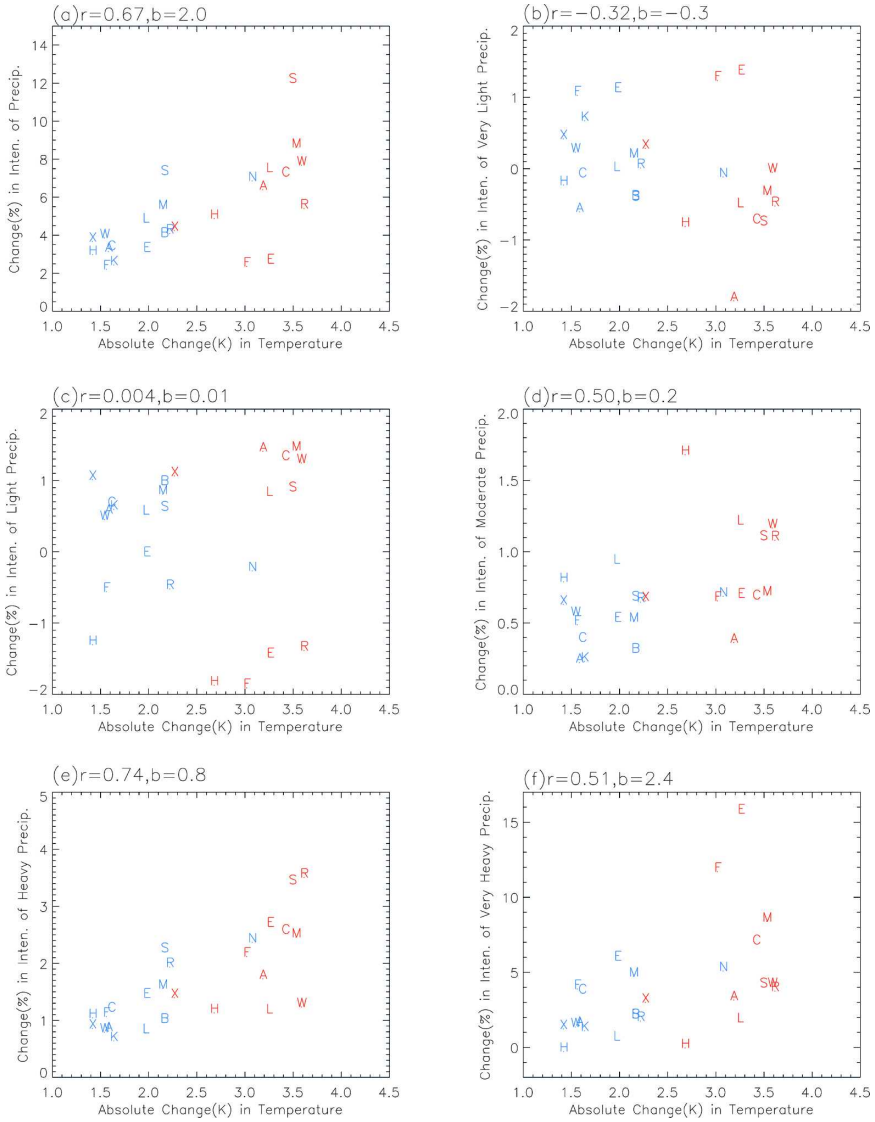

FIG. 5. Same as Fig. 3, but for the intensity of (a) all precipitation events, (b) very light, (c) light, (d) moderate, (e) heavy, and (f) very heavy precipitation.

(Fig. 5a). Combined with the decreases in precipitation frequency under SRES A2 (Fig. 4a), these two models produce smaller precipitation increases under SRES A2 than SRES B1 despite the larger warming for SRES A2 (Fig. 3a), which is an exception among all the models. Changes in the intensity of very light and light precipitation are within ±2% (Figs. 5b,c), whereas they are all positive for the intensity of moderate to very heavy precipitation for all the models, with the magnitude of the percentage change increasing with the mean intensity (Figs. 5d–f). Although variable from model to model, the intensity increases with global surface warming by about 0.8% K^{-1} for the heavy precipitation and by about 2.4% K^{-1} for very heavy precipitation. For precipitation events >100 mm day^{-1}, the intensity increases with temperature by 1.8% K^{-1} (not shown). These rates are much lower than the moisture change rate (~9.1% K^{-1}, see Fig. 3b) or the 7% K^{-1} implied by the simple thermodynamic consideration (Trenberth et al. 2003). This suggests that in most models the percentage increases in atmospheric water vapor are not fully transferred to percentage increases in precipitation intensity, as suggested by Trenberth et al. (2003). We recognize that the predefined intensity for the categorized events limit the magnitude of increases in the intensity (but not for the intensity for all precipitation events). More discussions on this are given in the last section.

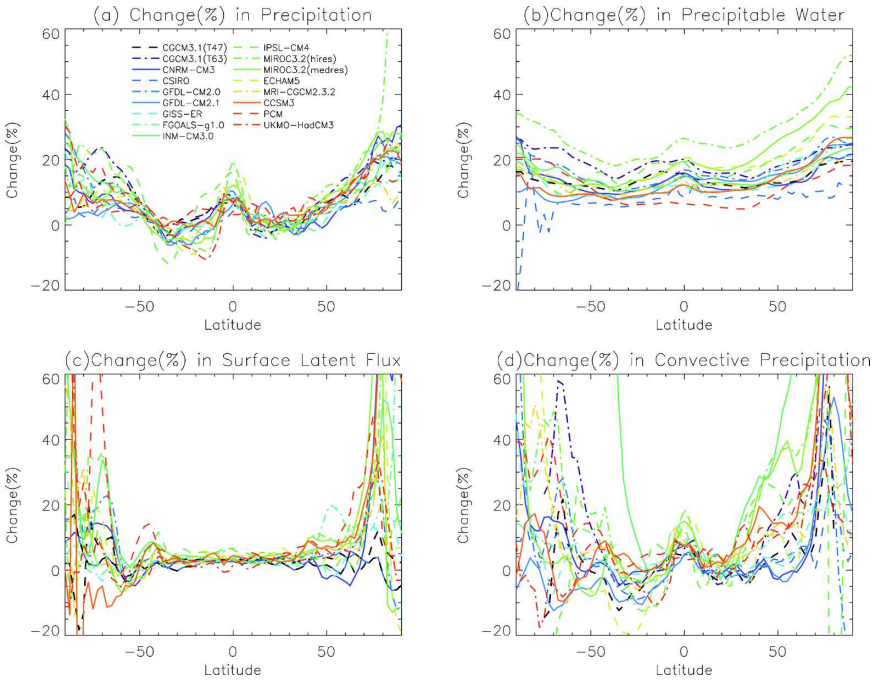

FIG. 6. Model-simulated future relative changes (%) from 1980–99 to 2080–99 in zonally averaged, annual-mean (a) precipitation amount, (b) precipitable water, (c) surface latent heat flux, and (d) convective precipitation for SRES B1.

5. Future changes in precipitation characteristics: Zonal mean

Figure 6 shows the percentage change in precipitation amount, precipitable water, surface latent heat flux, and convective precipitation amount from 1980–99 to 2080–99 for scenario SRES B1 (similar patterns for SRES A2). Consistent with previous studies (e.g., Cubasch et al. 2001; Dai et al. 2001a,b), precipitation amount increases in the Tropics and mid- and high latitudes and decreases or changes little in the subtropics in most of the models. Precipitable water increases at all latitudes for almost all the models, except for a fluctuation over southern high latitudes in the CSIRO model. Model MIROC3.2(hires) has the largest increase in precipitable water at all the latitudes, which is due to the very large warming in this model. The zonal distribution of changes in precipitable water is similar to that in temperature (not shown), reflecting the strong dependence of atmospheric moisture content on temperature (Dai 2006a). Very warm temperatures in MIROC3.2(hires) are associated with limited sea ice in the high-latitude Northern Hemisphere in this model (Zhang and Walsh 2006).

The surface latent heat flux generally exhibits an increase at all latitudes (Fig. 6c). In the Tropics and subtropics, the percentage increase is small (2%–7%) with relatively small intermodel spreads. The percentage increase is very large (>50%) at high latitudes for some of the models, but the small mean values at these latitudes should be noted in this context. This is also true for convective precipitation, which shows large percentage increases (>60%) in northern high latitudes for many of the models (Fig. 6d). In the Tropics and subtropics, the percentage change in convective precipitation is similar to that in total precipitation, with decreases in the southern subtropics. Note that the GFDL models show smaller changes in convective precipitation than most models at all the latitudes, especially in the Northern Hemisphere for SRES A2 (not shown), which explains the small increase in global-mean convective precipitation in these two models (Fig. 3d).

Figure 7 shows the percentage changes in the frequency of different categories of precipitation. For all types of precipitation events, most models show small frequency increases (≤2%) over the equator, small decreases (0%∼−4%) in the subtropics (20°–40°), and large increases (5%–20%) in the high latitudes. Model ECHAM5 shows much larger decreases in the subtropics than other models, which explains the large decrease for this model in global-mean precipitation frequency (cf. Fig. 4a). For very light precipitation, the frequency decreases around 65°S and over the equator for most models, whereas it increases at high latitudes but with

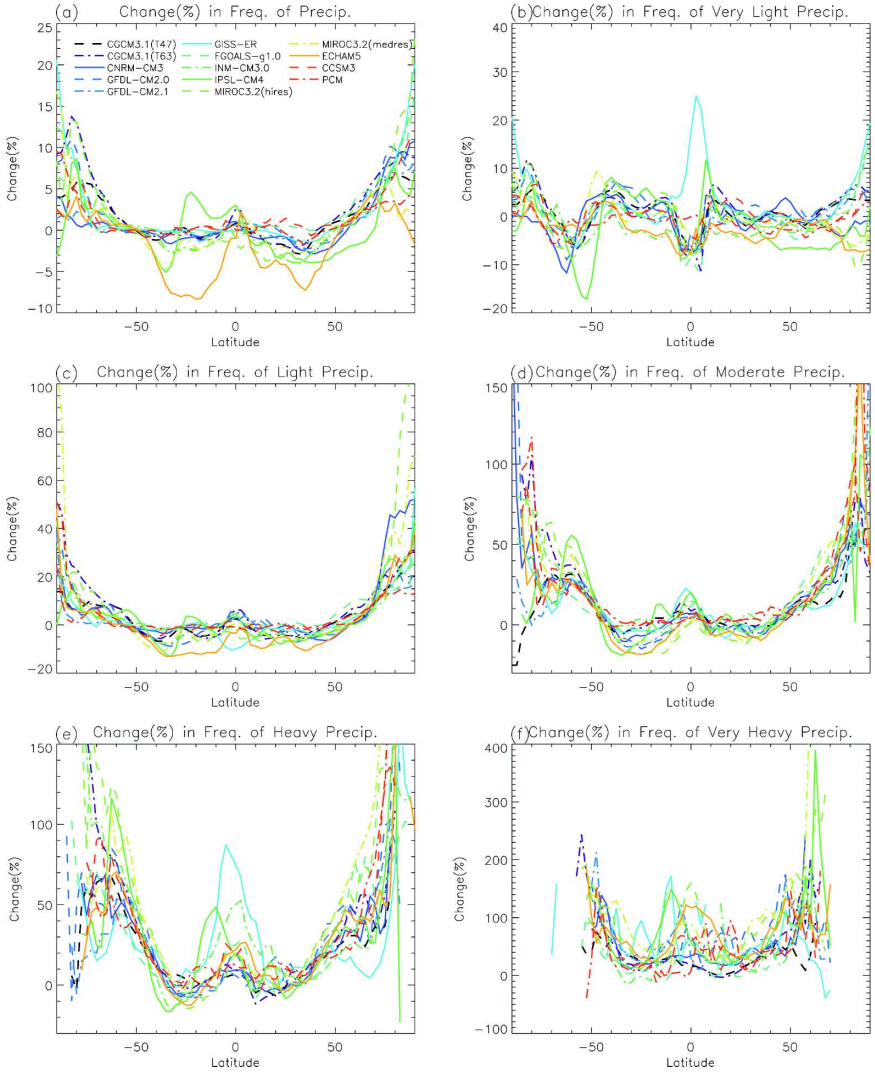

FIG. 7. Same as in Fig. 6, but for the frequency of (a) all precipitation events, (b) very light, (c) light, (d) moderate, (e) heavy, and (f) very heavy precipitation.

large spreads at the other latitudes. For light and moderate precipitation, the percentage frequency changes are fairly consistent among the models, with large increases in high latitudes, small decreases in the subtropics, and small increases in midlatitudes and over the equator. The amplitude of the percentage change for moderate precipitation is larger than for light precipitation. Figures 7e and 7f show that the frequency for heavy and very heavy precipitation increases at all latitudes except the subtropics in all the models. Many models show very large percentage increases in the frequency of very heavy precipitation in the Tropics (≥100%) and mid- and high latitudes (>400%). As mentioned above, the very large values in the high latitudes in Figs. 7d and 7f are related to the fact that moderate, heavy, and very heavy precipitation occurs infrequently in these regions in the current climate.

The intensity of all precipitation events increases by 5%–20% over the equator and mid- and high latitudes and changes little or decreases slightly over 15°–45°S and 5°–25°N (Fig. 8a). The longitudinal patterns of the changes in intensity of total and light precipitation are very similar (Figs. 8a,c) because of the large contribution of light precipitation to total precipitation. These patterns are also similar to the pattern of change in total precipitation amount (cf. Fig. 6a). For very light precipitation, the intensity changes are small except over the North Pole, where increases by 5%–20% are obtained in some of the models (Fig. 8b). The changes in the intensity of moderate and heavy precipitation are

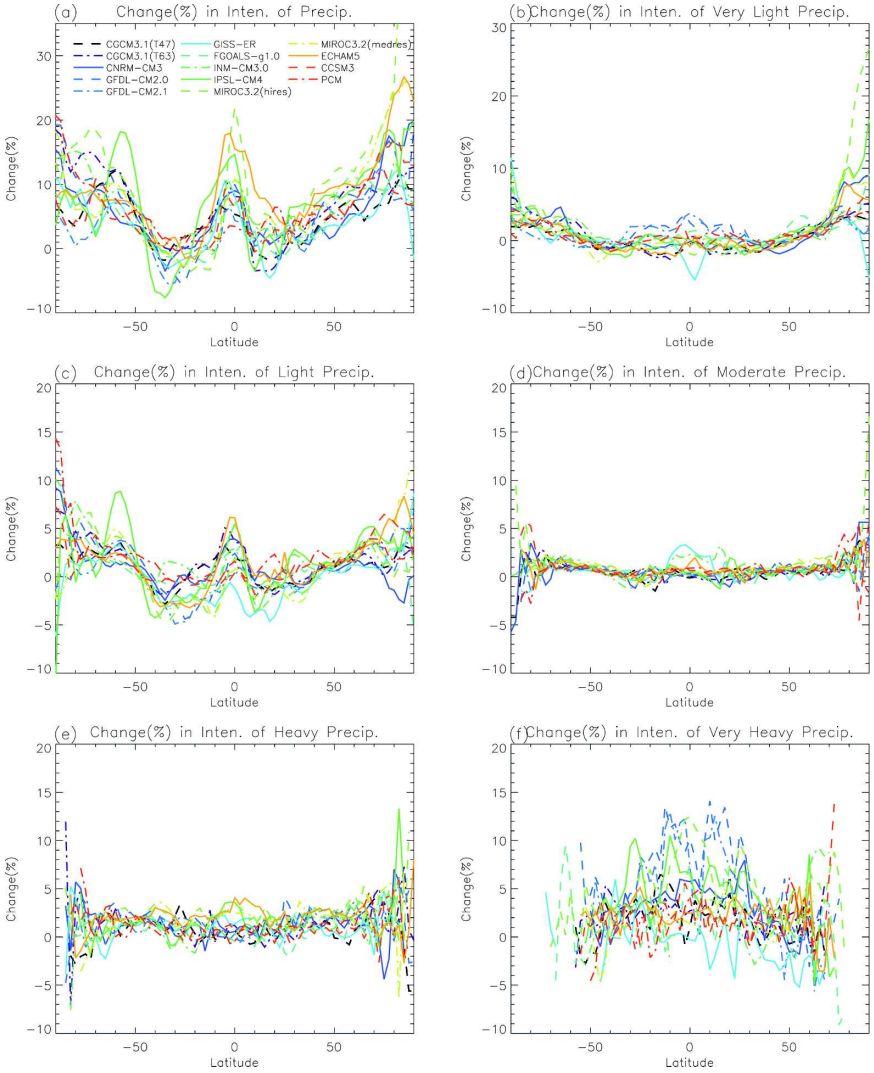

FIG. 8. Same as in Fig. 6, but for the intensity of (a) all precipitation events, (b) very light, (c) light, (d) moderate, (e) heavy, and (f) very heavy precipitation.

also small, within ±5% at most latitudes. The intensity change for very heavy precipitation is generally positive, with a large intermodel range of −5%–15% (Fig. 8f). It should be emphasized that the intensity changes are somewhat limited by the predefined rates of the precipitation categories (cf. section 2).

6. Future changes in precipitation characteristics: Geographical distribution

The geographical distributions of percentage change from 1980–99 to 2080–99 in precipitation amount, surface latent heat flux, precipitable water, and convective precipitation are shown in Fig. 9 as the 17-model arithmetic mean for SRES B1. Similar patterns are seen for SRES A2 (not shown), except that the magnitude of changes are larger due to increased radiative forcing. As mentioned above, percentage increases are large at high latitudes but the mean values are small in these regions. The precipitation change patterns shown in Fig. 9 are similar to those of previous studies (e.g., Cubasch et al. 2001). Precipitation amount increases by 10%–25% over the equatorial Pacific and by 5%–10% over northern mid- and high latitudes. Precipitation decreases (by 5%–10%) over most of the subtropical regions. Surface latent heat flux (i.e., evaporation) increases over most of the globe, except for the midlatitude North Atlantic, parts of the Southern Oceans, and a number of dry land areas, such as the Sahel, southern Africa, and the southwestern United States (Fig. 9b),

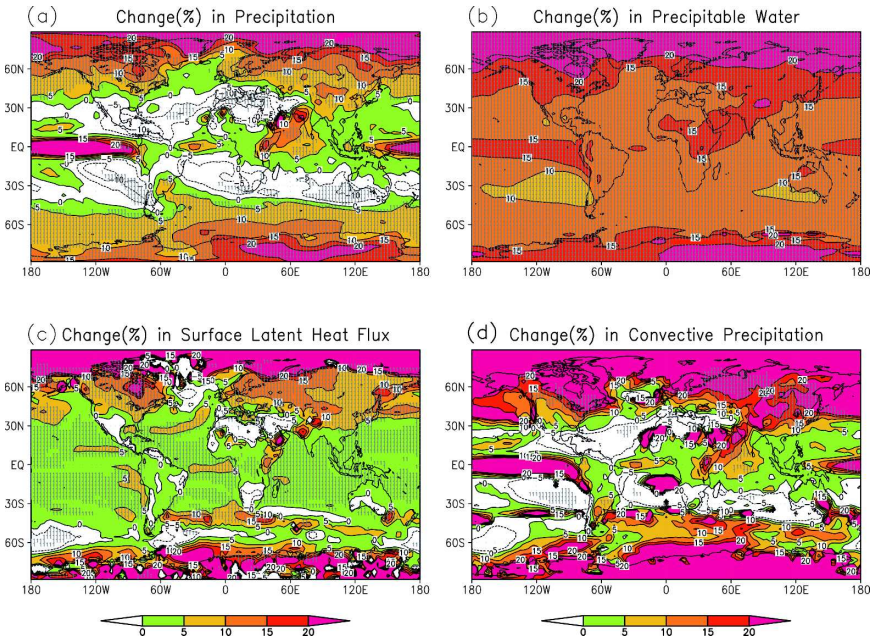

FIG. 9. Seventeen-model ensemble mean of future changes (%) from 1980–99 to 2080–99 under the SRES B1 scenario in annual-mean (a) precipitation amount, (b) precipitable water, (c) surface latent heat flux, and (d) convective precipitation. Gray stippling denotes areas where the magnitude of the multimodel ensemble mean exceeds the intermodel std dev.

where decreased precipitation (cf. Fig. 9a) is associated with reduced evaporation. PW increases by 10%–15% over most oceans and 15%–25% over most land areas (Fig. 9c). The ubiquitous increase in PW over the entire globe comes from its strong dependence on air temperature, which increases everywhere in the lower troposphere (not shown). The relatively large increases in PW over the equatorial Pacific and African–Indian monsoon regions (Fig. 9c) are accompanied by large increases in total and convective precipitation (Figs. 9a,d). Combined with the strong association between PW and precipitation increases at northern mid- and high latitudes (Figs. 9a,c), this suggests that local thermodynamics has a large effect on precipitation changes over these regions. This is consistent with Emori and Brown (2005) who found that thermodynamics plays a primary role in the change of mean precipitation over most of the globe. On the other hand, both the total and convective precipitation decreases over many subtropical regions, where PW also increases. This indicates that enhanced subsidence over these regions related to more vigorous tropical convection is likely to be a significant dynamic factor contributing to the decrease in mean precipitation over the subtropical regions. Emori and Brown (2005) found that the thermodynamic component of mean precipitation change over the subtropics decreases or changes little in the downward and/or weak upward motion regime over the subtropics, which also reflects the important role of atmospheric circulation changes.

Figure 10 shows the spatial distribution of changes in precipitation frequency for SRES B1 based on a 14-model ensemble since daily data are available only for 14 models. In most low and midlatitudes, precipitation events are less frequent in 2080–99 than the present. Over dry regions, such as northern Africa, the Arabian Peninsula, the western United States, and southern Australia, precipitation frequency decreases more (>5%) than other parts of the world. Since these regions are already dry, they could become more vulnerable to drought in 2080–99. Over the tropical Pacific, South Asian, and African monsoon regions and high latitudes, precipitation frequency increases. The percentage increase over Antarctica is large, but mean values are small there. The pattern of change for light precipitation frequency (Fig. 10c) is very similar to the change in all precipitation events because of the large contribution from light precipitation. The pattern for very light precipitation is slightly different from that for the other categories, with decreases of very light rainy days over the tropical Pacific, most land areas, and Southern Hemisphere high latitudes and increases over the southern subtropical oceans and Antarctica.

The frequency over the tropical Pacific and the Af-

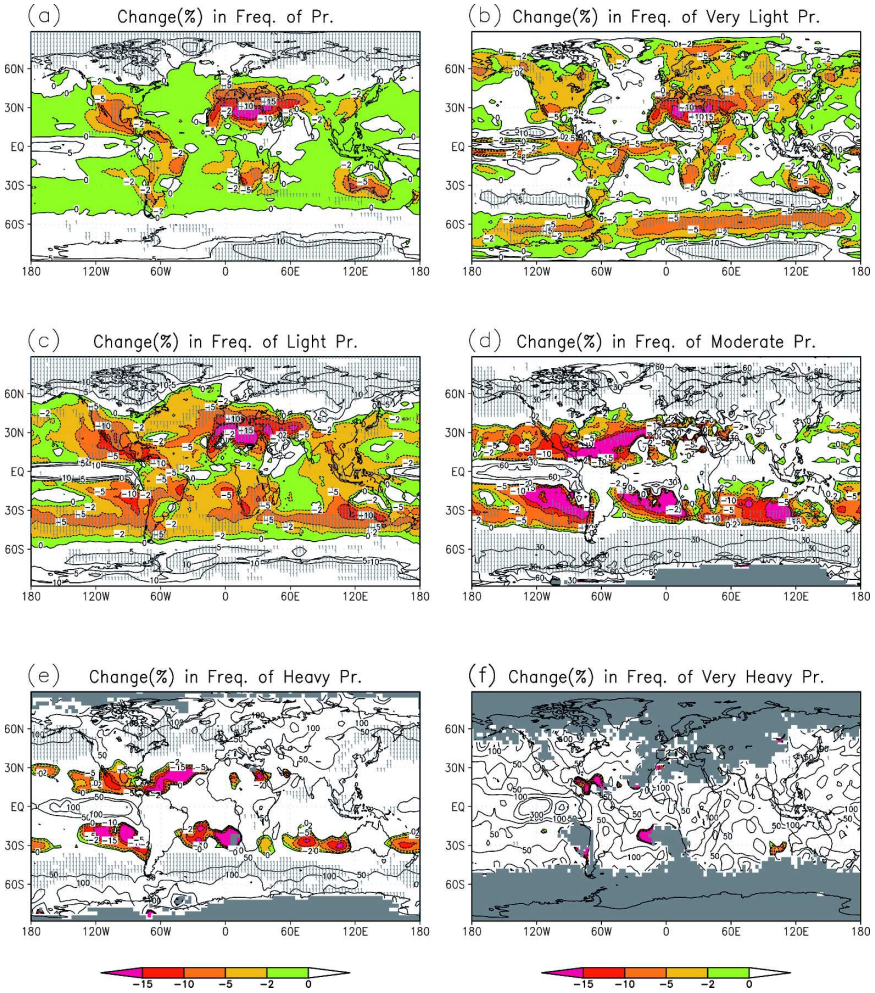

FIG. 10. Fourteen-model ensemble mean of changes (%) from 1980–99 to 2080–99 under the SRES B1 scenario in the annual-mean frequency of (a) all precipitation events, (b) very light, (c) light, (d) moderate, (e) heavy, and (f) very heavy precipitation. Gray stippling denotes areas where the magnitude of the multimodel ensemble mean exceeds the intermodel standard deviation. Gray shaded areas indicate that (d) moderate, (e) heavy, (f) and very heavy precipitation never occur there in all the considered models.

rican monsoon regions increases for all the categories except very light precipitation. For most of the Asian monsoon regions, the frequency increases in moderate, heavy, and very heavy precipitation but decreases in light and very light precipitation. Over the high latitudes and polar regions, the frequency generally increases for all the categories. The frequency decreases for light, moderate, and heavy precipitation over the southern subtropical oceans. Over many dry regions, such as northern Africa, the western United States, and southern Australia, all the categories of precipitation are less frequent in 2080–99 than the present.

The change in the intensity of all precipitation events (Fig. 11a) is similar to the change in precipitation amount (cf. Fig. 9a), as mentioned above. This is because the frequency changes are relatively small (Fig. 10a), and the precipitation amount changes come largely from the intensity changes. The intensity changes are large at high latitudes (in percentage terms) partly because of relatively small mean values of intensity there.

For very light and light precipitation, the intensity increases by ~2%–6% over the tropical oceans and high latitudes and decreases by ~1%–2% over the subtropical oceans. For moderate, heavy, and very heavy precipitation, the intensity increases over most of the globe by 2%–5%. Even for very heavy precipitation and precipitation >100 mm day^{-1} (not shown), the increase of intensity is only about 5% over most of the Tropics, which is smaller than the large increases

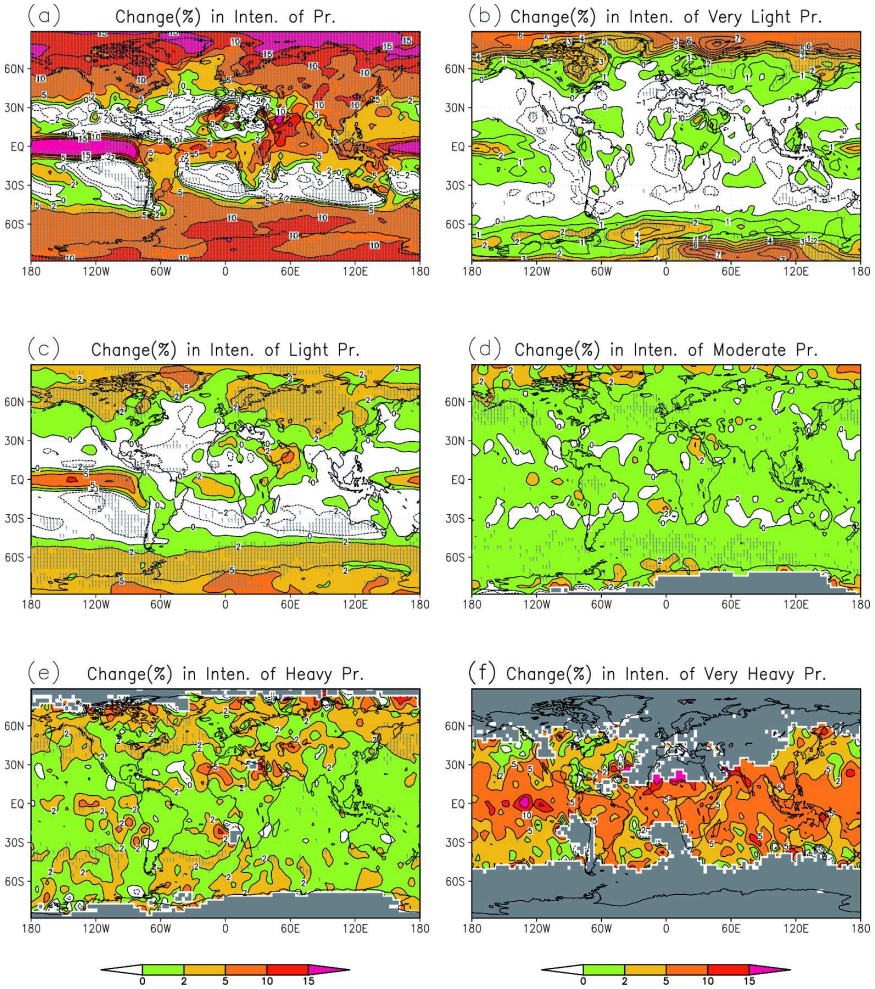

FIG. 11. Same as Fig. 9, but for the annual-mean intensity of (a) all precipitation events, (b) very light, (c) light, (d) moderate, (e) heavy, and (f) very heavy precipitation.

(>100%) in the frequency over the same regions. The frequency increase in heavy precipitation is enhanced by the shift of precipitation frequency distribution toward extreme events, while the large mean values of intensity for heavy precipitation events limit the percentage increases of the intensity.

Over regions with >10% increases in precipitation amount, such as high latitudes, the tropical Pacific, and South Asian and African monsoon regions, both the intensity and frequency increase in the warmer climates (Figs. 9a, 10a, and 11a). On the other hand, both the intensity and frequency decrease over some subtropical dry regions with >10% decreases in precipitation amount, such as northern Africa, the western United States, southern subtropical oceans, and Australia.

The qualitative consistency of the precipitation changes among the models was examined. The largest intermodel difference can be seen in changes in convective precipitation (Fig. 9d), frequency, and intensity of heavy and very heavy precipitation (Figs. 10e,f and 11e,f), indicating the high uncertainty in simulating and projecting these variables. Most models show qualitatively consistent changes over the regions with large changes in precipitation frequency and intensity, such as high latitudes, parts of the tropical Pacific and Asian and African monsoon regions, and the Sahel. However, over regions where the magnitude of change is small, model results may differ even in the sign of change. In addition, except high latitudes, the regions with a good model agreement in precipitation change are also those with good model agreement in changes of very light and light precipitation frequency (cf. Figs. 10 and 11a). This implies that the consistent precipitation change over these regions is owing to models' consistent behavior in simulating changes for very light and light precipitation.

7. Discussion and conclusions

Under the SRES B1, A1B, and A2 emissions scenarios examined here, precipitation histograms in all the models show a shift toward the right-hand side from 1980–99 to 2080–99, indicating more intense and less light precipitation. For both the SRES B1 and A2 emissions scenarios, all 17 models examined show increases in global-mean precipitation amount and intensity, precipitable water, and surface evaporation. Most models show a decrease of global precipitation frequency under SRES A2, a high emissions scenario, but more than half of the models do not show decreased global-mean precipitation frequency under SRES B1, a low emissions scenario. This is mainly because the regional response increases with increased radiative forcing. The model results are qualitatively consistent with the theoretical conjecture that precipitation intensity will increase at a faster rate than precipitation amount at the expense of precipitation frequency in a warmer climate (Trenberth et al. 2003).

The multimodel ensemble results show a global-mean precipitation increase of about 1.2% K^{-1} during the twenty-first century, which is similar to previous estimates (e.g., Cubasch et al. 2001). They also show an increase of ~9.1% K^{-1} in global precipitable water and an increase of ~2.0% K^{-1} in global precipitation intensity but a decrease of ~0.7% K^{-1} in global precipitation frequency under both the SRES B1 and A2 scenarios. The change in precipitable water has the best linear relationship with temperature change, and the increasing rate is slightly higher than that estimated from the Clausius–Clapeyron equation (~7%, see Trenberth et al. 2003). This discrepancy may partly result from the extra contribution from the reduction in the tropospheric temperature lapse rate in the Tropics under global warming (Bony et al. 1995). The increase of precipitation intensity is much larger than the decrease of the frequency, which reflects the fact that the increase in precipitation amount is due to an increase in precipitation intensity partly offset by a decrease in precipitation frequency. However, the increase in the frequency of very heavy precipitation is much larger than those in their intensity. This suggests that there could be considerably more frequent heavy precipitation events in 2080–99 than the present, but their intensity may not change greatly in percentage terms in a warmer climate. The frequency increase in heavy precipitation is enhanced by the shift of precipitation frequency distribution toward extreme events, while the large mean values of intensity for heavy precipitation events limit the percentage increases of the intensity. Furthermore, the high emissions scenario SRES A2 shows the largest shift toward heavy precipitation and the largest decrease in precipitation frequency, which implies an increased risk of floods and droughts for many regions with the large increase of greenhouse gases.

The model-predicted global-mean increase of precipitation intensity (~2.0% K^{-1}) is considerably smaller than that estimated from the simple thermodynamics by Trenberth et al. (2003), who suggested that storm intensity should increase roughly at the same rate as atmospheric water vapor (~7% K^{-1}). The smaller increase of intensity is consistent with Emori and Brown (2005) who found that the precipitation increase resulting from thermodynamics is smaller than the increase in extreme precipitation (which is comparable to increases in atmospheric water vapor) over certain areas. Many factors could contribute to the apparent discrepancy between the model results and simple thermodynamics. For example, the rate of ~7% K^{-1} for precipitable water may not apply to precipitation generated from nonconvective events, which are important, especially in mid- and high latitudes during the cold season (Dai 2001; Dai 2006b). Also, the neglect of the role of atmospheric circulation and regional variations in the simple thermodynamic calculation may contribute to the quantitative difference. The shift toward heavier precipitation events likely plays an important role for the model-simulated intensity changes. On the other hand, the poor performance of current climate models in simulating the frequency and intensity of precipitation outside the 10–20 mm day^{-1} category (Sun et al. 2006; Dai 2006b) is also a likely factor. Furthermore, precipitation intensity defined in this paper is based on daily precipitation totals that could be lower than actual value because precipitation often occurs only during part of the day. This may be one reason why the change in precipitation intensity is less than that based on simple thermodynamics.

Geographical distributions based on multimodel ensembles also show some interesting results. Over currently wet regions, such as the tropical Pacific Ocean, South Asian, and African monsoon regions, precipitation amount, frequency, and intensity are all projected to increase for all precipitation events as a whole and for almost all precipitation categories. An exception is East and Southeast Asian monsoon regions, where the total precipitation intensity increases but total frequency decreases. However, the frequency for heavy and very heavy precipitation increases over these regions, indicating that the increase in precipitation amount in these regions is mainly due to the shift toward heavier precipitation. Over currently dry areas, such as northern Africa, the western United States, Australia, and southern subtropical oceans, precipita-

tion amount, frequency, and intensity all decrease for all precipitation categories. This indicates that under future warming scenarios, wet regions may get wetter and dry regions may become drier mostly because of simultaneous increase (decrease) of total precipitation frequency and intensity. Furthermore, our results show that the percentage changes in all the precipitation-related variables over the polar regions are much larger than over other areas (e.g., Cubasch et al. 2001). Although the large changes partly result from the small mean values there, this reflects the vulnerability and large climate sensitivity over the polar regions under global warming.

Acknowledgments. This research was partially done while the first author held a National Research Council Research Associateship Award at Aeronomy Laboratory, NOAA, Boulder, Colorado. We thank three anonymous reviewers for helpful comments and suggestions and Pingping Xie for providing the data. We acknowledge the international modeling groups for providing their data for analysis, the Program for Climate Model Diagnosis and Intercomparison (PCMDI) for collecting and archiving the model data, the JSC/CLIVAR Working Group on Coupled Modelling (WGCM) and their Coupled Model Intercomparison Project (CMIP) and Climate Simulation Panel for organizing the model data analysis activity, and the IPCC WG1 TSU for technical support. The IPCC Data Archive at Lawrence Livermore National Laboratory is supported by the Office of Science, U.S. Department of Energy. And thanks also go to Roy Miller, Barb Keppler, and John Daniel for helpful suggestions. Y. Sun is partially supported by Chinese NSF Grant 40605020 and 973 program 2006CB403604. A. Dai is partially supported by the NCAR Water Cycle Program and by NSF Grant ATM-0233568.

REFERENCES

Allen, M. R., and W. J. Ingram, 2002: Constraints on the future changes in climate and the hydrological cycle. *Nature,* **419,** 224–232.

Boer, G. J., 1993: Climate change and the regulation of the surface moisture and energy budgets. *Climate Dyn.,* **8,** 225–239.

Bony, S., J. P. Duvel, and H. L. Treut, 1995: Observed dependence of the water vapor and clear-sky greenhouse effect on sea surface temperature: Comparison with climate warming experiments. *Climate Dyn.,* **11,** 307–320.

Chen, M., R. E. Dickinson, X. Zeng, and A. N. Hahmann, 1996: Comparison of precipitation observed over the continental United States to that simulated by a climate model. *J. Climate,* **9,** 2223–2249.

Cubasch, U., and Coauthors, 2001: Projections of future climate change. *Climate Change 2001: The Scientific Basis,* J. T. Houghton et al., Eds., Cambridge Unversity Press, 525–582.

Dai, A., 2001: Global precipitation and thunderstorm frequencies. Part I: Seasonal and interannual variations. *J. Climate,* **14,** 1092–1111.

——, 2006a: Recent climatology, variability and trends in global surface humidity. *J. Climate,* **19,** 3589–3606.

——, 2006b: Precipitation characteristics in eighteen coupled climate models. *J. Climate,* **19,** 4605–4630.

——, F. Giorgi, and K. E. Trenberth, 1999: Observed and model simulated precipitation diurnal cycles over the contiguous United States. *J. Geophys. Res.,* **104,** 6377–6402.

——, T. M. L. Wigley, B. A. Boville, J. T. Kiehl, and L. E. Buja, 2001a: Climates of the twentieth and twenty-first centuries simulated by the NCAR Climate System Model. *J. Climate,* **14,** 485–519.

——, G. A. Meehl, W. M. Washington, T. M. L. Wigley, and J. M. Arblaster, 2001b: Ensemble simulation of twenty-first century climate changes: Business-as-usual versus CO_2 stabilization. *Bull. Amer. Meteor. Soc.,* **82,** 2377–2388.

Emori, S., and S. J. Brown, 2005: Dynamic and thermodynamic changes in mean and extreme precipitation under changed climate. *Geophys. Res. Lett.,* **32,** L17706, doi:10.1029/2005GL023272.

——, A. Hasegawa, T. Suzuki, and K. Dairaku, 2005: Validation, parameterization dependence, and future projection of daily precipitation simulated with a high-resolution atmospheric GCM. *Geophys. Res. Lett.,* **32,** L06708, doi:10.1029/2004GL022306.

Gordon, H. B., P. H. Whetton, A. B. Pittock, A. M. Fowler, and M. R. Haylock, 1992: Simulated changes in daily rainfall intensity due to the enhanced greenhouse effect: Implications for extreme rainfall events. *Climate Dyn.,* **8,** 83–102.

Groisman, P. Y., R. W. Knight, T. R. Karl, D. R. Easterling, B. M. Sun, and J. H. Lawrimore, 2004: Contemporary changes of the hydrological cycle over the contiguous United States: Trends derived from in situ observations. *J. Hydrometeor.,* **5,** 64–85.

——, ——, D. R. Easterling, T. R. Karl, G. C. Hegerl, and V. A. N. Razuvaev, 2005: Trends in intense precipitation in the climate record. *J. Climate,* **18,** 1326–1350.

Haylock, M., and N. Nicholls, 2000: Trends in extreme rainfall indices for an updated high quality data set for Australia, 1910–1998. *Int. J. Climatol.,* **20,** 1533–1541.

Hennessy, K. J., J. M. Gregory, and J. F. B. Mitchell, 1997: Changes in daily precipitation under enhanced greenhouse conditions. *Climate Dyn.,* **12,** 667–680.

Karl, T. R., and R. W. Knight, 1998: Secular trends of precipitation amount, frequency, and intensity in the United States. *Bull. Amer. Meteor. Soc.,* **79,** 231–241.

Klein Tank, A. M. G., and G. P. Können, 2003: Trends in indices of daily temperature and precipitation extremes in Europe, 1946–99. *J. Climate,* **16,** 3665–3680.

Kunkel, K. E., D. R. Easterling, K. Redmond, and K. Hubbard, 2003: Temporal variations of extreme precipitation events in the United States: 1895–2000. *Geophys. Res. Lett.,* **30,** 1900, doi:10.1029/2003GL018052.

Manton, M. J., and Coauthors, 2001: Trends in extreme daily rainfall and temperature in Southeast Asia and the South Pacific: 1961-1998. *Int. J. Climatol.,* **21,** 269–284.

Meehl, G. A., J. M. Arblaster, and C. Tebaldi, 2005: Understanding future patterns of precipitation extremes in climate model simulations. *Geophys. Res. Lett.,* **32,** L18179, doi:10.1029/2005GL023680.

Semenov, V. A., and L. Bengtsson, 2002: Secular trends in daily precipitation characteristics: Greenhouse gas simulation with a coupled AOGCM. *Climate Dyn.,* **17,** 123–140.

Shepard, D., 1968: A two-dimensional interpolation function for regularly spaced data. *Proc. 23d National Conf. of American Computing Machinery,* Princeton, NJ, Association for Computing Machinery, 517–524.

Soden, B. J., R. T. Wetherald, G. L. Stenchikov, and A. Robock, 2002: Global cooling after the eruption of Mount Pinatubo: A test of climate feedback by water vapor. *Science,* **296,** 727–730.

Sun, Y., S. Solomon, A. Dai, and R. W. Portmann, 2006: How often does it rain? *J. Climate,* **19,** 916–934.

Tebaldi, C., K. Hayhoe, J. M. Arblaster, and G. A. Meehl, 2006: Going to the extremes: An intercomparison of model-simulated historical and future changes in extreme events. *Climatic Change,* **79,** 185–211.

Trenberth, K. E., 1998: Atmospheric moisture residence times and cycling: Implications for rainfall rates with climate change. *Climatic Change,* **39,** 667–694.

——, A. Dai, R. M. Rasmussen, and D. B. Parsons, 2003: The changing character of precipitation. *Bull. Amer. Meteor. Soc.,* **84,** 1205–1217.

Watterson, I. G., and M. R. Dix, 2003: Simulated changes due to global warming in daily precipitation means and extremes and their interpretation using the gamma distribution. *J. Geophys. Res.,* **108,** 4379, doi:10.1029/2002JD002928.

Wilby, R. L., and T. M. L. Wigley, 2002: Future changes in the distribution of daily precipitation totals across North America. *Geophys. Res. Lett.,* **29,** 1135, doi:10.1029/2001GL013048.

Xie, P., B. Rudolf, U. Schneider, and P. A. Arkin, 1996: Gauge-based monthly analysis of global land precipitation from 1971 to 1994. *J. Geophys. Res.,* **101,** 19 023–19 034.

Zhang, X., and J. E. Walsh, 2006: Toward a seasonally ice-covered Arctic Ocean: Scenarios from the IPCC AR4 model simulations. *J. Climate,* **19,** 1730–1747.